Electronic structure and optical response of L-$CePd_5$

A. Vega,* S. Bouarab, and M. A. Khan
Institut de Physique et Chimie des Matériaux de Strasbourg, 23 rue du Loess, 67037 Strasbourg, France
(Received 26 July 1994; revised manuscript received 7 October 1994)

A theoretical study of the electronic structure and the related optical response of L-$CePd_5$ is reported. The charge distribution is calculated self-consistently within the linear muffin-tin-orbital method in the atomic-sphere approximation. The exchange and correlation potential is treated in the local-density approximation. The origin of the different electronic states is discussed in terms of the hybridization between the Ce and Pd orbitals, and is illustrated by means of the l-projected local density of states at each inequivalent atom within the unit cell. The different electronic population at each inequivalent site is analyzed as a function of the local coordination number as well as by considering the chemical character of the neighboring atoms. The different absorption peaks obtained in the imaginary part of the dielectric function and in the real part of the optical conductivity are traced back to particular interband transitions. A comparison of the present results with those for other Ce-Pd alloys is made.

I. INTRODUCTION

In the past years, a considerable effort has been invested both from the experimental and theoretical points of view in order to understand the electronic properties and, in particular, the optical response in the Ce-Pd intermetallic compounds. Most of the exciting properties exhibited by the ordered Ce-Pd alloys are due to the $4f$ states of Ce, which are in the vicinity of the Fermi energy (E_F) and, thus, strongly hybridize with the conduction $4d$ band of the neighboring Pd atoms. The relative position of the resulting electronic states depends not only on the concentration of Ce and Pd in the corresponding alloy, but also in the particular geometrical arrangement of the atoms, and confers to these materials a fluctuating valence character. Moreover, the geometrical order in these materials has been observed to vary as a function of the annealing temperature[1–3] and pressure.[4] This has an influence in properties like the electrical resistivity which increases significantly with pressure.[5]

Spectroscopic measurements have been performed for $CePd_3$ by Allen *et al.*[6] and Peterman *et al.*[7] from which the valence-band photoemission spectra have been obtained. The empty states have been observed through bremsstrahlung isochromat spectroscopy (BIS) by Hillebrecht *et al.*[8] With respect to $CePd_7$, the same properties have been studied through BIS, core level x-ray-photoemission spectroscopy and x-ray-absorption spectroscopy by Beaurepaire *et al.*[9] Besides, measurements of magnetic susceptibility and specific heat have been recently reported for this system.[10–12] The theoretical calculations for these compounds through the linear augmented plane wave (LAPW) method (Refs. 13 and 14) and through linear muffin-tin orbital (LMTO) (Refs. 15 and 9) present a rather good agreement with the above experimental observations. In the case of $CePd_5$, most of the experimental efforts have been devoted to the study of the electrical resistivity[1] and the crystal structure[2,3] as a function of the annealing temperature. However, up to now, no experimental results concerning the electronic structure and optical properties are available for this system. In order to have a unified picture over the Ce-Pd alloys, these properties deserve to be also investigated in $CePd_5$. It is the aim of this work to present a detailed theoretical study of the electronic and optical properties of this alloy, and to compare the general trends obtained with those for $CePd_3$ and $CePd_7$.

The rest of the paper is organized as follows. After a brief account, in Sec. II, of the crystal structure of $CePd_5$, we will present in Sec. III the theoretical model used for the calculations. The discussion of the results for the electronic distribution and optical response is reported in Secs. IV and V, respectively. Section VI summarizes the results.

II. GEOMETRICAL STRUCTURE

The crystal structure of $CePd_5$ has been recently analyzed through x-ray diffraction by Kuwano *et al.*[2,3] It is revealed that this compound has two phases, one stable at low temperature (L-$CePd_5$), and the other at high temperature (H-$CePd_5$). The structure of L-$CePd_5$ is regarded as orthorhombic with lattice parameters $a = 0.5700$ nm, $b = 0.4062$ nm and $c = 0.8461$ nm. The numbers of cerium and palladium sites in the unit cell are two and ten, respectively. In Fig. 1, the unit cell is illustrated and the coordinates of the twelve atoms are given. By taking into account the different local environment of each atom, i.e., the local coordination number and the chemical character of the neighboring sites, five different types of atoms can be found within the unit cell. The two Ce atoms are equivalent (type 1) and there are four types of Pd atoms: types 2, 4, and 5 with two atoms in each case, and type 3 with four atoms.

Site	coordinates	type
Ce	(1/2,0,1/3)	1
Ce	(0,0,2/3)	1
Pd	(0,0,0)	2
Pd	(1/2,0,0)	2
Pd	(1/4,1/2,1/6)	3
Pd	(3/4,1/2,1/6)	3
Pd	(1/4,1/2,5/6)	3
Pd	(3/4,1/2,5/6)	3
Pd	(0,0,1/3)	4
Pd	(1/2,0,2/3)	4
Pd	(1/4,1/2,1/2)	5
Pd	(3/4,1/2,1/2)	5

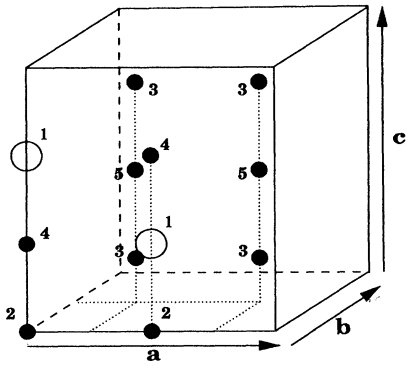

a=0.5700nm b=0.4062nm c=0.8461nm

FIG. 1. The twelve atoms of the unit cell are illustrated, together with the coordinates in the orthorhombic crystal and the different types of sites. The Wigner-Seitz radius is 2.9748 a.u.

III. THEORETICAL MODEL

The electronic structure from which the optical properties are to be calculated, has been determined self-consistently within the LMTO method in the atomic-sphere approximation (ASA).[16,17] The charge distribution for the isolated atoms of the two species has been calculated self-consistently by solving the relativistic Dirac equation.[18] These core states are then kept frozen in the compound. The starting atomic potential is constructed with $4f^2 5d^0 6s^2$ for Ce, and $4d^{10} 5s^0$ for Pd as the valence electrons. Since the $4f$ electrons of Ce in the Ce-Pd alloys are known to be in the vicinity of the Fermi energy (E_F), most of the exciting properties expected for this compound will come from the hybridization between these localized states and the conduction d band. This effect is expected to have an important influence in the electronic redistribution (charge transfer) and in the optical response of the system. In spite of the above facts, the $4f$ electrons have been considered as valence electrons explicitly in the self-consistent calculation. Since for narrow band the third-order LMTO method is only valid in a relatively narrow energy interval around the center of gravity,[16,17] special attention has been focused in obtaining the $4f$-valence electrons within the energy window, where the expansion of the muffin-tin orbitals is accurate enough.

The exchange and correlation potential has been treated in the local-density approximation (LDA), within the von Barth–Hedin approximation.[19] Although the many-body effects play generally an important role in the localized states, it is now well established that as far as the $4f$ states in the Ce-Pd alloys are nearly empty and they affect essentially through hybridization, the LDA approximation for these states, as for the other valence states, gives rather good results.[13,14] Previous calculations for $CePd_3$ (Ref. 15) and $CePd_7$ (Ref. 9) within the LMTO-ASA model have lead to rather satisfactory agreement with experimental observations.[7,20] Finally, the combined correction to the ASA (Ref. 16) has been taken into account in the calculations. All the integrations in the Brillouin zone have been performed by using the tetrahedron technique[21,22] with 125 k points within 1/8 of the Brillouin zone.

IV. ELECTRONIC DISTRIBUTION

The total density of states within the unit cell is plotted in Fig. 2. The occupied part is characterized by three regions of high density. In the unoccupied part, two regions of high density are obtained. Figure 3 exhibits the partial, orbital-projected local densities of states at each inequivalent site within the unit cell. A comparison with

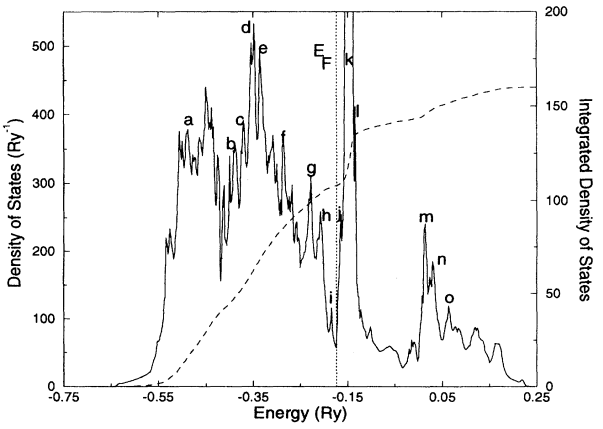

FIG. 2. Total density of states (continuous line) and integrated number of states (dashed line) per unit cell ($2CePd_5$). E_F denotes the Fermi level.

Fig. 2 allows us to explain the origin of the different structures obtained in the total density of states, and to illustrate the hybridization and l character of each particular state. The occupied part has mainly the $4d$ character from the Pd atoms, and a small amount of (Pd) sp and (Ce) d character in the lowest energy region. Hybridization between (Pd) d and (Ce) f states takes place also in the occupied part near E_F. The three high-density structures of the occupied part are clearly identified in the local density of states of the Pd atoms of type 2.

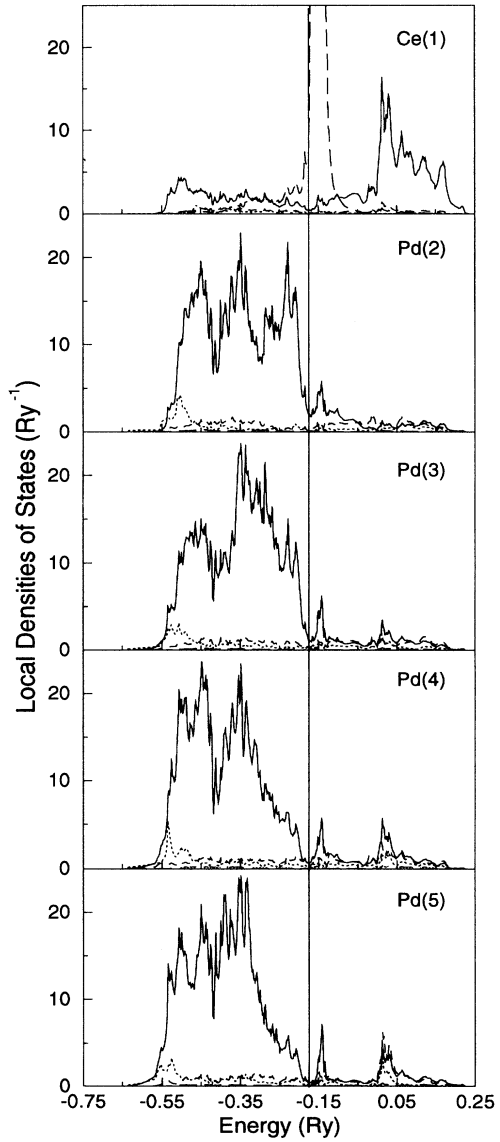

FIG. 3. The orbital-projected local densities of states at each inequivalent atom within the unit cell. The dotted line corresponds to the s symmetry, the dashed line to the p symmetry, the solid line to the d symmetry, and the long-dashed line to the f symmetry.

These atoms are characterized by a local neighborhood in which only one Ce nearest neighbor is present and the rest of nearest neighbors are atoms of Pd. Thus, the local density of states resembles that of pure Pd. However, as the relative number of Ce neighbors in the local environment of the different Pd atoms increases, we observe a tendency to a narrowing of the corresponding local densities of states, together with the vanishing of the occupied high-density region near the E_F. This is particularly clear in the Pd atoms of types 4 and 5 having three and four Ce nearest neighbors, respectively. The presence of such high number of Ce in their neighborhood gives rise to a reduction of the covalent bonding and as a consequence of the narrowing of the local density of states and an increase of the electronic occupation is obtained, as discussed below. With respect to the unoccupied part, the first large peak above E_F is due mainly to the $4f$ electrons of Ce, although some hybridization with the unbonded $4d$ states of Pd can be observed. A comparison with $CePd_3$ (Ref. 15) and $CePd_7$ (Ref. 9) reveals a shift of this localized $4f$ peak towards the Fermi energy when the concentration of Ce increases in the compound. Finally, the second peak in the empty region has the Ce d character and s, p, and d contributions from the Pd atoms mainly of type 4 and 5 and to a small amount of type 3.

The hybridization effects have a strong influence on the resulting local electronic occupations. In Table I, the results are reported for the number of valence electrons (N_l^σ) per spin (σ) for the different orbitals (l) at each of the five inequivalent sites within the system. The density of states at the Fermi energy ($\sum_l n_l^\sigma(E_F)$) as well as the charge transfer (ΔQ / atom) are also given. For the sake of comparison, we have included within the table the corresponding values for $CePd_3$ and $CePd_7$ taken from previous works.[15,9] We obtain a charge transfer from the Ce atoms towards the Pd neighbors. The same trend was obtained for the other two compounds. The total valence-electronic occupation obtained in each Ce atom of $CePd_5$ is $2.884e^-$. Therefore, the Ce atoms are more like trivalent, as in the case of $CePd_3$ ($2.880e^-$) and $CePd_7$ ($2.876e^-$). The excess of electrons in the Pd atoms (calculated within the Wigner-Seitz sphere of R_{WS} = 2.9748 a.u.) depends on the local geometrical and chemical environment of each of the four types. In particular, it can be directly related to the number of Ce atoms in their neighborhood. Thus, the Pd atoms of types 2, 3, 4, and 5 have one, two, three, and four Ce first neighbors, respectively, so that the gain of electrons coming from these Ce atoms increases from $0.078e^-$ in Pd (2) to $0.186e^-$ in Pd (3), $0.269e^-$ in Pd (4), and $0.397e^-$ in Pd (5). This trend can be verified by comparing the departure from the local neutrality of the Pd atoms of type 3 in $CePd_5$ (ΔQ/atom = $-0.186e^-$) with that of Pd atoms of type 3 in $CePd_7$ (ΔQ/atom= $-0.173e^-$). In these two cases, both Pd atoms have two Ce neighbors and a similar ΔQ/atom. The same holds for Pd (5) in $CePd_5$ (ΔQ/atom= $-0.397e^-$) and Pd (2) in $CePd_3$ (ΔQ/atom= $-0.372e^-$), which have four Ce neighbors.

For the Fermi density contribution in Table I, we have presented the total density of states at E_F for three

TABLE I. Orbital-projected electronic occupations (N_l^σ), local densities of states at the Fermi energy ($\sum_l n_l^\sigma(E_F)$), and the departure from the local neutrality (ΔQ/ atom). The corresponding results for $CePd_3$ and $CePd_7$, taken from Refs. 14 and 15, respectively, are included for the sake of comparison. σ denotes the spin and $l = s, p, d, f$ the orbital quantum number. ($\star$) For $CePd_3$, the authors have given only the total density of states per unit cell at the Fermi level.

	N_s^σ	N_p^σ	N_d^σ	N_f^σ	$\sum_l N_l^\sigma$	$\sum_l n_l^\sigma(E_F)$	ΔQ/atom
$CePd_5$							
Ce(1)	0.108	0.110	0.728	0.495	1.442	10.369	1.116
Pd(2)	0.318	0.303	4.371	0.047	5.039	2.440	−0.078
Pd(3)	0.325	0.318	4.404	0.046	5.093	3.107	−0.186
Pd(4)	0.350	0.344	4.393	0.047	5.135	1.294	−0.269
Pd(5)	0.384	0.344	4.433	0.047	5.198	1.245	−0.397
$CePd_7$							
Ce(1)	0.108	0.109	0.601	0.619	1.438	7.355	1.123
Pd(2)	0.312	0.316	4.370	0.045	5.042	5.425	−0.085
Pd(3)	0.325	0.293	4.426	0.041	5.086	3.905	−0.173
$CePd_3$							
Ce(1)	0.138	0.110	0.589	0.603	1.440	13.56*	1.117
Pd(2)	0.361	0.323	4.458	0.043	5.185		−0.372

compounds. For $CePd_3$, the authors[15] have given many possible values under different conditions of calculations. So in the table, we have given the value which corresponds to the present model of calculation. The specific heats measurements[23,10–12] confirm the general trends of $n(E_F)$ in the case of $CePd_3$ and $CePd_7$. Unfortunately, such measurements in the case of $CePd_5$ are still lacking.

V. OPTICAL RESPONSE

Once the self-consistent energy bands are obtained, the optical response can be easily calculated. The optical absorption is directly proportional to the imaginary part of the dielectric function $\varepsilon(\omega) = \varepsilon_1(\omega) + i\varepsilon_2(\omega)$, ω being the photon frequency.[24] The function $\varepsilon_2(\omega)$ incorporates two terms: one term, $\varepsilon_2^f(\omega)$, which accounts for intraband transitions (Drude's term), and another term, $\varepsilon_2^b(\omega)$, corresponding to interband transitions, which is calculated in the present work. In the limit of zero linewidth (infinite lifetime of the states), the interband term has the following expression at $T = 0$ K:

$$\varepsilon_2^b(\omega) = \frac{e^2}{2\pi m^2\omega^2}\sum_{n,n'}\int_{\omega_{nn'}(\vec{k})=\hbar\omega}\frac{|\,\hat{e}\cdot\vec{P}_{nn'}(\vec{k})\,|^2}{|\,\vec{\nabla}\omega_{nn'}(\vec{k})\,|}d\vec{S}_k. \tag{1}$$

Here, n and n' indicate the occupied and empty bands, respectively. The unit vector in the photon direction is denoted by $\hat{e}$, and $\vec{P}_{nn'}(\vec{k})$ is the dipole matrix element between the states $|\,n\vec{k}\rangle$ and $|\,n'\vec{k}\rangle$. The integration is performed within the region of the Brillouin zone where $\omega_{nn'}(\vec{k}) = E_{n'}(\vec{k}) - E_n(\vec{k}) = \hbar\omega$.

For an orthorhombic material, the contributions to the dielectric function from the different directions have, according to the above expression, the following form:

$$\varepsilon_2^{b,(i)}(\omega) = \frac{e^2}{2\pi m^2\omega^2}\sum_{n,n'}\int_{\omega_{nn'}(\vec{k})=\hbar\omega}\frac{|\,P_{nn'}^{(i)}(\vec{k})\,|^2}{|\,\vec{\nabla}\omega_{nn'}(\vec{k})\,|}d\vec{S}_k \tag{2}$$

for $i = x, y, z$. The total optical absorption is, then, calculated as

$$\varepsilon_2^{b,(T)}(\omega) = \varepsilon_2^{b,(x)}(\omega) + \varepsilon_2^{b,(y)}(\omega) + \varepsilon_2^{b,(z)}(\omega). \tag{3}$$

Although we determine the dielectric function by means of the wave functions calculated for the ground state, it has been established in preceding works[25–31] that the LMTO method gives good agreement with experimental data, particularly in the low-energy range.

More related with experiments is the real part of the optical conductivity, $\sigma_1^{b,(T)}(\omega) = \omega\varepsilon_2^{b,(T)}(\omega)/4\pi$. The results for $\varepsilon_2^{b,(T)}(\omega)$ and $\sigma_1^{b,(T)}(\omega)$ are plotted in Figs. 4 and 5, respectively. One can see the rich peak structure obtained through the band calculation. This is partly due to the fact that the structure of $CePd_5$ is composed of five inequivalent atoms within an orthorhombic crystal, so that each component of the dielectric function $[\varepsilon_2^{b,(i)}(\omega), i = x, y, z]$ at each inequivalent atom contributes differently to the total optical absorption spectrum. In Table II, the energies corresponding to the different absorption peaks for $CePd_5$ are reported, together with those obtained for $CePd_3$ in previous calculations.[15]

A comparison with $CePd_3$ reveals the richer peak structure in the case of $CePd_5$, particularly in the low-energy region ($\hbar\omega < 0.20$ Ry). However, due to the finite lifetime of the states, not all the peaks obtained in the calculations are expected to be observed in future experiments. For instance, in the low-energy region, we expect the peaks C, D, E, and probably I to be observed. In the high-energy region, J and K (which could appear as a

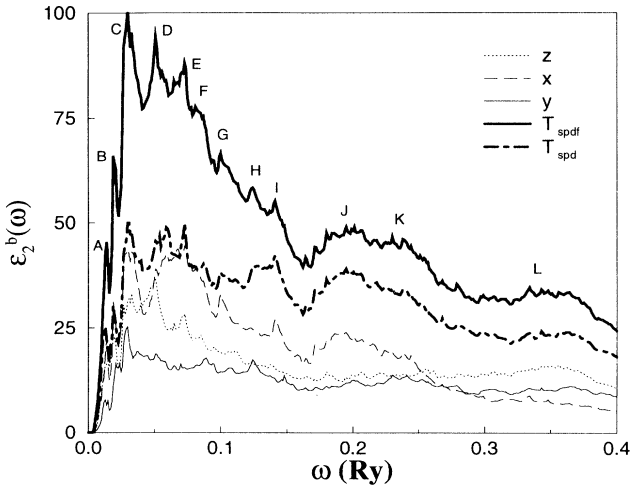

FIG. 4. The imaginary part of the dielectric function, $\varepsilon_2^{b,(T)}(\omega)$ versus ω. Thick solid line (T_{spdf}) presents $\varepsilon_2^{b,(T)}(\omega)$ when all the transitions (*spdf*) are taken into account while the thick dash-dot-dash (T_{spd}) presents the case when the $d \rightarrow f$ ($f \rightarrow d$) transitions are ignored. The x, y, and z contributions are also plotted.

unique broad peak in the experiment), and L should also be characterized. The origin of the different absorption peaks can be traced back to particular interband transitions as indicated in Table II. The significant high-density regions, which play an important role in interband transitions are indicated by small letters in Fig. 2. The peak C has its origin mainly in $d \rightarrow f$ transitions in Ce, and $p \rightarrow d$ and $d \rightarrow p$ transitions in Pd atoms of types 2 and 3. The states from which these transitions occur can be identified in the total density of states (Fig. 2). Thus,

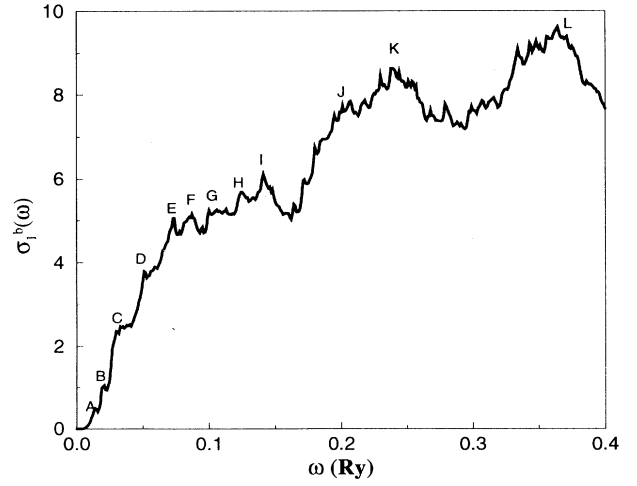

FIG. 5. The real part of the optical conductivity, $\sigma_1^{b,(T)}(\omega)$ versus ω. $\sigma_1^{b,(T)}$ is expressed in Ry (1 Ry = 3.2885 × 10^{15} sec^{-1}).

TABLE II. The optical peak positions (in eV) for $CePd_5$. The values in parenthesis for $CePd_3$, taken from Ref. 14, are included for the sake of comparison. Some of the peaks of the total density of states corresponding to the most relevant absorption peaks, as explained in the text, are also reported.

	Peak positions											
	A	*B*	*C*	*D*	*E*	*F*	*G*	*H*	*I*	*J*	*K*	*L*
	0.20	0.27	0.48	0.68	1.02	1.16	1.36	1.70	1.90	2.72	3.26	4.76
		(0.24)	(0.47)	(0.77)		(1.06)			(2.67)		(2.81)	(4.55)
			$i \rightarrow j$	$h \rightarrow j$	$g \rightarrow j$				$f \rightarrow k$	$d \rightarrow k$	$b \rightarrow k$	$a \rightarrow k$
				$i \rightarrow k$	$h \rightarrow k$						$c \rightarrow l$	$e \rightarrow m$
											$i \rightarrow m$	$f \rightarrow o$
											$h \rightarrow n$	

the position of the absorption peak C corresponds to the energy between the peak labeled i and the one labeled j. The peak D is attributed also to $d \rightarrow f$ transitions in Ce, and $p \rightarrow d$ and $d \rightarrow p$ in Pd atoms mainly of type 2 [peaks (h,j) and (i,k) in the total density of states]. The absorption peaks E and I have their origin mainly in $d \rightarrow f$ and $f \rightarrow d$ transitions in Ce, and $p \rightarrow d$ and $d \rightarrow p$ in Pd atoms of all types [peaks (g,j) and (h,k) in the total density correspond to E, and (f,k), for instance, corresponds to I].

As we approach to higher-energy regions, we find an increasing broadening of the corresponding peaks due to the fact that more transitions are possible from the numerous occupied $d(p)$ states towards the unoccupied $p(d)$ states of Pd. Finally, in the high-energy region ($\hbar\omega > 0.20$ Ry), considerable broad J, K, and L peaks are obtained. We attribute their origin to (Ce) $d \rightarrow f$ and (Ce) $f \rightarrow d$ transitions as well as to (Pd) $d \rightarrow p$ and (Pd) $p \rightarrow d$ transitions. In the case of $CePd_3$, in the high-energy region the corresponding peaks were noted as E, F, and G in Ref. 15, and they lie at somewhat lower energies than the corresponding J, K, and L peaks in $CePd_5$. In Ref. 15, these structures were attributed to mainly (Pd) $d \rightarrow p$ transitions. Later, Koenig and Knab[31] after a detailed study came to the same conclusion that these peaks were mainly due to (Pd) $p \rightarrow d$ transitions and the contribution from (Ce) $d \rightarrow f$ transitions was found to be negligible. These theoretical results were in contradiction to the explanations given by Hillebrands *et al.*,[20] where they invoked the possibility of intersite (Pd) $d \rightarrow$ (Ce) f transitions. But this idea was put forward before the energy bands of $CePd_3$ were calculated. In the present case of $CePd_5$, the peaks J, K, and L are predominatly due to the (Pd) $d \rightarrow p$ transitions with some contribution of (Ce) $d \rightarrow f$. To check the part played by the (Ce) $d \rightarrow f$ transitions, we have switched off these transitions in the calculations of $\varepsilon_2^b(\omega)$. Thus, we obtain the results where f state is totally ignored. The result is shown by a thick dash-dot-dash curve in Fig. 4. When we compare these results with thick continuous curve where $d \rightarrow f$ transitions are included, we see that in the low-energy range the $d \rightarrow f$ transition is almost as important as *sp* and *pd* transitions, whereas in the high-energy range, the contribution is mainly due to *pd* transitions with a small contribution of $d \rightarrow f$ transitions.

In the general expression (2), the term $\mid P_{nn'}(\vec{k}) \mid^2$ contains different kinds of contributions. When one is dealing with only s and p states, $\mid P_{nn'}(\vec{k}) \mid^2$ is composed of the following terms:

$$\begin{aligned} \mid P_{nn'}(\vec{k}) \mid^2 = & \mid P^{sp}_{nn'}(\vec{k}) \mid^2 + \mid P^{ps}_{nn'}(\vec{k}) \mid^2 \\ & + 2[(P^{sp}_{nn'}(\vec{k}))_R \times (P^{ps}_{nn'}(\vec{k}))_R \\ & + (P^{sp}_{nn'}(\vec{k}))_I \times (P^{ps}_{nn'}(\vec{k}))_I]. \end{aligned} \tag{4}$$

$P^{sp}_{nn'}(\vec{k})$ is the dipole matrix element when the s symmetry of the initial state $\mid n\vec{k}\rangle$ and the p symmetry of the final state $\mid n'\vec{k}\rangle$ are involved. The subscripts R and I stand for real and imaginary parts. The first two terms which we call the direct components, are always positive, whereas the last term which we call indirect contribution may be positive or negative. The corresponding total $\varepsilon_2^{sp}(\omega)$ will contain all these terms, but it is easy to obtain the parts played by the different contributions. When *spdf* states are involved, one can decompose $\varepsilon_2(\omega)$ as follows:

$$\varepsilon_2^{spdf}(\omega) = \varepsilon_2^{spd}(\omega) + \varepsilon_2^{df}(\omega) + \varepsilon_2^{spd-df}(\omega). \tag{5}$$

$\varepsilon_2^{spd}(\omega)$ is the total contribution of the direct as well as indirect terms of all *spd* states. In this situation, the indirect terms also involve the contributions like $2[(P^{sp}_{nn'}(\vec{k}))_R \times (P^{pd}_{nn'}(\vec{k}))_R + \cdots]$, as well as $2[(P^{pd}_{nn'}(\vec{k}))_R \times (P^{dp}_{nn'}(\vec{k}))_R + \cdots]$ along with the last term in Eq. (4). $\varepsilon_2^{df}(\omega)$ is due to the direct and indirect contributions of the *df* states. The last term is the cross contribution of *spd* and *df*. In Fig. (4), we have given the total $\varepsilon_2^{spdf}(\omega)$ and $\varepsilon_2^{spd}(\omega)$. To see how important the other terms are, we show in Fig. 6 all the four terms in expression (5). At low energy, $\varepsilon_2^{spd-df}(\omega)$ has appreciable negative as well as positive contributions, whereas at $\hbar\omega > 0.10$ Ry it fluctuates around zero. Though it is a nice theoretical exercise to dissect the total $\varepsilon_2^b(\omega)$ into the relevent components, unfortunately, these sophisticated details cannot be verified experimentally.

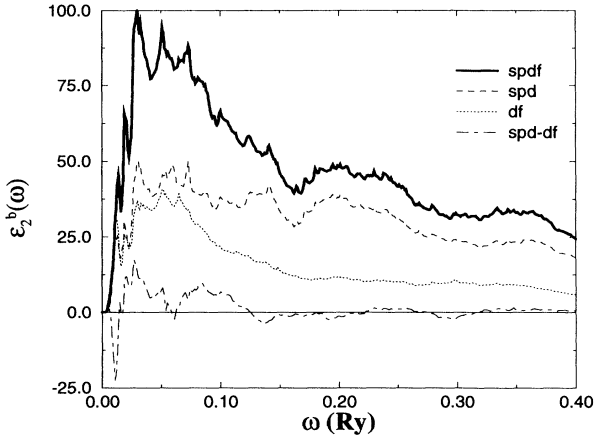

FIG. 6. The imaginary part of the dielectric function, $\varepsilon_2^{b,(T)}(\omega)$ versus ω : total contribution of *spdf* (thick solid line), contribution of *spd* (dashed line), contribution of *df* (dotted line), and the cross contribution *spd-df* (dot-dashed line).

VI. CONCLUSION

The self-consistent band-structure calculation for L-$CePd_5$ gives an electronic distribution with three high-density regions in the occupied part, which come mainly from the $4d$ band of the Pd atoms that hybridizes with the $4f$ electrons of Ce near the Fermi energy. The Fermi energy lies in a pseudogap very close to the very localized $4f$ states of Ce which hybridize, as well, with the unbonded $4d$ electrons of Pd. An electronic charge transfer from the Ce atoms towards the Pd neighbors is obtained

and differs for each atom depending on its local neighborhood. Similar behaviors have been obtained in the other Ce-Pd alloys. A rich structure for the optical absorption spectrum has been obtained, particularly in the low-energy region. The different peaks have been traced back to particular interband transitions. The outcome of the present theoretical work awaits experimental confirmation. But, since the agreements between calculated values[15] and the experimental observations[32,33,8,34] for $CePd_3$ and for $CePd_7$ (Ref. 9) are good, we expect future experiments on $CePd_5$ to confirm the general features of the electronic structure and optical spectrum presented in this work.

ACKNOWLEDGMENTS

A. Vega would like to acknowledge the Ministerio de Educación y Ciencia (Spain) for a post-doctoral grant and the IPCMS-GEMM group for their kind hospitality. We are thankful to Drs. J. P. Kappler, E. Beaurepaire, and J. C. Parlebas for many discussions.

*On leave from Departamento de Física Teórica, Facultad de Ciencias, Universidad de Valladolid, 47011 Valladolid, Spain

[1]M. Itakura, N. Kuwano, and K. Oki, J. Alloys Comp. **192**, 245 (1993).

[2]N. Kuwano, K. Umeo, K. Yamamoto, M. Itakura, and K. Oki, J. Alloys Comp. **181**, 61 (1992).

[3]N. Kuwano, S. Higo, K. Yamamoto, K. Oki, and T. Eguchi, Jpn. J. Appl. Phys. **24**, 663 (1985).

[4]T. P. Beales, A. H. Presland, M. Doyle, I. R. Harris, and D. W. Jones, J. Less-Common Met. **158**, 35 (1990).

[5]K. Umeo, Y. Aya, M. Itakura, N. Kuwano, and K. Oki, J. Phys. Chem. Solids **54**, 131 (1993).

[6]J. W. Allen, S. J. Oh, I. Lindau, J. M. Lawrence, L. J. Johnsson, and S. B. M. Hangström, Phys. Rev. Lett. **46**, 1100 (1981).

[7]D. J. Peterman, J. H. Weaver, and M. Croft, Phys. Rev. B **25**, 5530 (1982).

[8]F. U. Hillebrecht, J. C. Fuggle, G. A. Sawatzky, and R. Zeller, Phys. Rev. Lett. **51**, 1187 (1983).

[9]E. Beaurepaire, J. P. Kappler, S. Lewonczuk, J. Ringeissen, M. A. Khan, J. C. Parlebas, Y. Iwamoto, and A. Kotani, J. Phys. Condens. Matter **5**, 5841 (1993).

[10]J. P. Kappler, M. J. Besnus, P. Lehmann, A. Meyer, and J. G. Sereni, J. Less-Common Met. **3**, 261 (1985).

[11]J. G. Sereni, O. Trovarelli, J. Schaf, G. Schmerber, and J. P. Kappler, Mod. Phys. Lett. B **5**, 1249 (1991).

[12]J. G. Sereni, O. Trovarelli, A. Herr, J. P. Schillé, E. Beaurepaire, and J. P. Kappler, J. Phys. Condens. Matter **5**, 2927 (1993).

[13]D. D. Koelling, Solid State Commun. **43**, 247 (1982).

[14]D. D. Koelling (unpublished).

[15]C. Koenig and M. A. Khan, Phys. Rev. B **38**, 5887 (1988).

[16]O. K. Andersen, Phys. Rev. B **12**, 3060 (1975).

[17]H. L. Skriver, *The LMTO Method* (Springer, Berlin, 1984).

[18]J. P. Desclaux, Comput. Phys. Commun. **9**, 31 (1975).

[19]U. von Barth and L. Hedin, J. Phys. C **5**, 1629 (1972).

[20]B. Hillebrands, G. Güntherodt, R. Pott, W. König, and A. Breitschwert, Solid State Commun. **43**, 891 (1982).

[21]O. Jepsen and O. K. Andersen, Solid State Commun. **9**, 1763 (1971).

[22]G. Lehman and M. Taut, Phys. Status Solidi B **54**, 469 (1972).

[23]M. J. Besnus, J. P. Kappler, and A. Meyer, J. Phys. F **13**, 597 (1983).

[24]D. Pines, *Elementary Excitations in Solids* (Benjamin, New York, 1964), p. 211.

[25]M. Alouani, C. Koenig, and M. A. Khan, Solid State Commun. **65**, 327 (1988).

[26]C. Koenig and M. A. Khan, Phys. Rev. B **27**, 6129 (1983).

[27]M. A. Khan, C. Koenig, and R. Riedinger, J. Phys. F **13**, L159 (1983).

[28]M. Alouani and M. A. Khan, J. Phys. (Paris) **47**, 453 (1986).

[29]M. Alouani, J. M. Koch, and M. A. Khan, J. Phys. F **16**, 473 (1986).

[30]N. I. Kulikov, M. Alouani, M. A. Khan, and M. V. Magnitskaya, Phys. Rev. B **36**, 929 (1987).

[31]C. Koenig and D. Knab, Solid State Commun. **74**, 11 (1990).

[32]J. Schoenes and K. Andres, Solid State Commun. **42**, 359 (1982).

[33]J. W. Allen, R. J. Nemanich, and S. J. Oh, J. Appl. Phys. **53**, 2145 (1982).

[34]B. C. Webb, J. A. Sievers, and T. Mihalisin, Phys. Rev. Lett. **57**, 1951 (1986).